Flexural and Shear Strength of Composite Lintels in Glass-Fiber-Reinforced Gypsum Wall Constructions

Y.-F. Wu[1] and M. P. Dare[2]

Abstract: Composite lintels are formed above the door and window openings of glass-fiber-reinforced gypsum (GFRG) wall constructions. These lintels are constructed by filling reinforced concrete into the hollow cores of the GFRG walls. The GFRG panel itself is a composite material composed of gypsum plaster and the reinforcing glass fiber. When filled with reinforced concrete the structural action of the lintels is derived from further composite action between the GFRG panel and the infill concrete. Experimental beam testing was conducted to study the flexural and shear behavior of these composite lintels. Typical failure modes and corresponding ultimate strengths were obtained and analyzed. Based on the test results, theoretical design models and guidelines are proposed for both the flexural and shear strengths.

DOI: 10.1061/(ASCE)0899-1561(2006)18:3(415)

CE Database subject headings: Composite materials; Glass fibers; Fiber reinforced materials; Gypsum; Flexural strength; Shear strength; Walls.

Introduction

A new composite walling product of glass-fiber-reinforced gypsum (GFRG), known as Rapidwall, is finding more and more applications in the building industry in Australia and a few Asian countries. GFRG walls are constructed using precast hollow panels that are machine made from formulated gypsum plaster and reinforced with chopped glass fibers. The typical cross section of the GFRG panel is shown in Fig. 1. In the manufacturing process 300–350 mm long glass fibers are randomly distributed inside the panel skins and in the ribs joining the skins. The fiber volume in the panel is about 0.8 kg/m^2 of wall area. The properties of the glass fiber are given in Table 1.

The physical properties of the current standard GFRG panels are provided in Table 2. The test methods used to determine these physical properties are described in the work by Wu (2002). More details of this product and its application can be found in the works of Wu (2002), Wu and Dare (2004), and Wu (2004). The GFRG panels are generally used as wall material to provide habitable enclosures in residential, commercial, and industrial buildings. The panels are made to one standard size. In the factory each GFRG panel is mechanically cut to size to include doors and windows in accordance with the construction drawings. The cut wall components are then transported to the construction site on trucks and erected using cranes, as shown in Fig. 2. Therefore, construction using GFRG wall panels is similar to construction using precast reinforced-concrete panels. However, weighing only 42 kg/m^2, the GFRG panels are considerably lighter than precast concrete panels. The cavities (hollow cores) within the GFRG panel can be filled with various materials including concrete, loose aggregates, or insulation materials, depending on the intended use. For instance, adding concrete will increase the structural strength of the wall and insulation will alter its thermal- and noise-attenuating properties.

The remaining part of GFRG panels above a window or a door opening is often used as lintel in constructions, as illustrated in Fig. 2. Reinforced concrete is filled into the cavities of a lintel to form a structural member similar to a reinforced concrete beam. Steel bars are inserted into the bottom of the lintel to form the tension reinforcement of the beam. Construction details of a typical lintel are shown in Fig. 3. This lintel construction produces a composite member that is made up of GFRG panel, infill concrete, and steel reinforcement. As a result, the conventional reinforced concrete theory may not be directly applicable to the design of such structural members. Experimental testing was carried out in order to study the behavior and develop design guidelines of the composite lintels, which are reported in this paper.

Composite Mechanism of the Lintels

Lintels are designed to resist both flexural moment and shear force. Obviously both the GFRG panel and the infill reinforced concrete contribute to the strengths of the composite lintels. In order to form a reinforced concrete beam, reinforcing bars are driven into the GFRG panel through the ribs from the end of the lintel, as shown in Figs. 3 and 4. This reinforcement is designed to provide tensile resistance to the concrete beam. By removing part of the ribs on top of the lintel as shown in Figs. 3 and 4, the concrete in the upper part of the lintel, which is in compression under bending, is continuous throughout the beam without being separated by the ribs of the GFRG panel. The continuity of con-

[1]Assistant Professor, Dept. of Building and Construction, City Univ. of Hong Kong, Tat Chee Ave., Kowloon, Hong Kong (corresponding author). E-mail: yfwu00@cityu.edu.hk

[2]Director, Dare Sutton Clarke Engineers, 276 Flinders St., Adelaide, South Australia 5000, Australia. E-mail: mpdare@dscgroup.net

Note. Associate Editor: Houssam A. Toutanji. Discussion open until November 1, 2006. Separate discussions must be submitted for individual papers. To extend the closing date by one month, a written request must be filed with the ASCE Managing Editor. The manuscript for this paper was submitted for review and possible publication on November 22, 2004; approved on March 25, 2005. This paper is part of the ***Journal of Materials in Civil Engineering***, Vol. 18, No. 3, June 1, 2006. ©ASCE, ISSN 0899-1561/2006/3-415–423/$25.00.

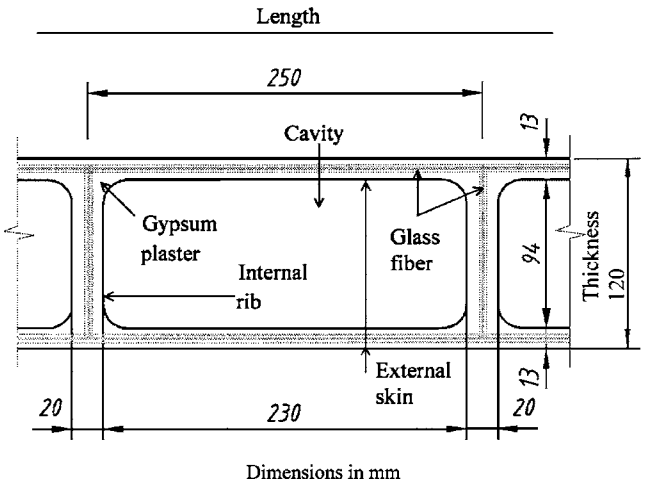

Fig. 1. Cross section of GFRG panel

crete in the compression zone is necessary to provide adequate compressive resistance in the reinforced concrete beam, because the compressive strength of the gypsum ribs is insufficient.

Similar to the flexural mechanism, the shear resistance also comes from two parts: the GFRG panel and the infill RC beam. Because the GFRG panel is reinforced with glass fibers, the tensile resistance of the glass fibers inside the GFRG panel is able to prevent diagonal shear cracking in the GFRG panel. By analogy to the function of stirrups in conventional RC beams, the function of the glass fibers in the GFRG panel can be seen as web reinforcement of the composite lintels.

Test Specimens

Details of the test specimen are shown in Fig. 4 and Table 3. The specimens had three different depths of 300, 550, and 800 mm, and five different span lengths of 0.6, 1.2, 1.8, 2.4, and 3.0 m. The total number of specimens was 18. Concrete infill for all the specimens was cast in one batch. The GFRG specimens were cut from randomly selected sample panels. One Y12 reinforcing bar was driven into the bottom of each specimen from the end of the GFRG panel, as shown in Fig. 4. Before placing the concrete into the GFRG panel, part of the ribs at the top of the lintel was cut off to provide a continuous concrete compression zone (see Fig. 4). The removed part of a rib was 150-mm deep by 94-mm wide.

To emulate actual construction practice the GFRG specimens were erected vertically, and self-compacting concrete was filled from the top of the lintel. Concrete cylinders (100-mm diameter by 200-mm height) were made from the same batch of concrete in order to identify the concrete strength. The age of concrete at the time of lintel tests was between 96 to 118 days, and the average concrete strength of the concrete cylinders was 21.3 MPa. Low-grade concrete is usually used for GFRG wall constructions. The reason is that the axial and shear strengths of the concrete-filled GFRG walls are not governed by the concrete strength, and higher strength of concrete is unnecessary (Wu and Dare 2004).

Table 1. Physical Properties of Glass Fiber

Property	Unit	Specification
Product: E glass fiber gun roving		E glass > 98%
Linear weight of roving	(tex)	2,400/5%
Sizing agent		Silane < 2%
Moisture	%	<0.20
Tensile strength	MPa	112
Tensile modulus	MPa	13,177
Flexural strength	MPa	321
Flexural modulus	MPa	13,149

Table 2. Physical Property of GFRG Panel

Property name	Value	Note
Compressive strength	⩾160 kN/m	Unfilled single leaf GFRG panel
Tensile strength	⩾35 kN/m	
Elastic modulus	3,000–6,000 MPa	
Unit weight	40 kg/m^2	
Thermal expansion coefficient	12×10^{-6} mm/mm/degrees C	
Water absorption	<5%	By weight after 24 h immersion
Thermal resistance	0.36 m^2 K/W	Unfilled panel
	1.63 m^2 K/W	With 35 kg/m^3 and R2.5 rockwool batts infill and standard texture finishing
Sound transmission coefficient (STC)	28	Unfilled panel
	45	Concrete-filled panel
Fire resistance level (FRL)	>3 h	For structural adequacy

Test Setup

The test setup is shown in Fig. 5. A spreader beam system was used to distribute the point load F from the loading jack into four equal point loads to simulate a uniformly distributed load. In order to prevent local crushing, steel C channels were placed under the point loads and at the supports that spread the point load to a larger area to prevent local crushing, as shown in Fig. 5. Immediately before attaching the C channels onto the specimen, a thick coat of quick-setting plaster was applied onto the three contact faces of the specimen to fill the gaps so that a full and firm contact between the C channels and the specimen was ensured.

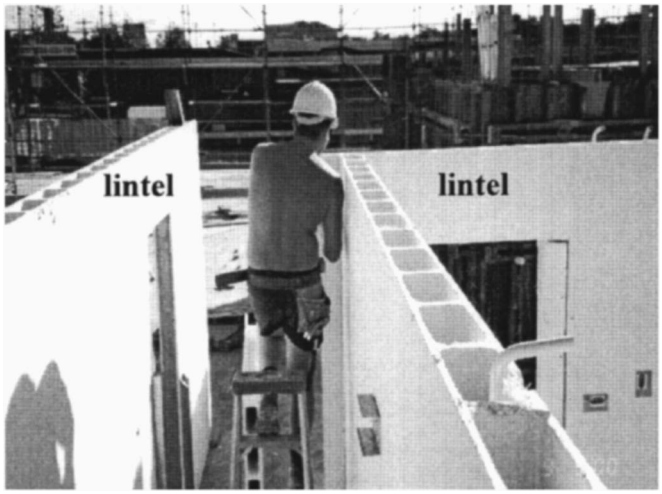

Fig. 2. Construction of GFRG wall building

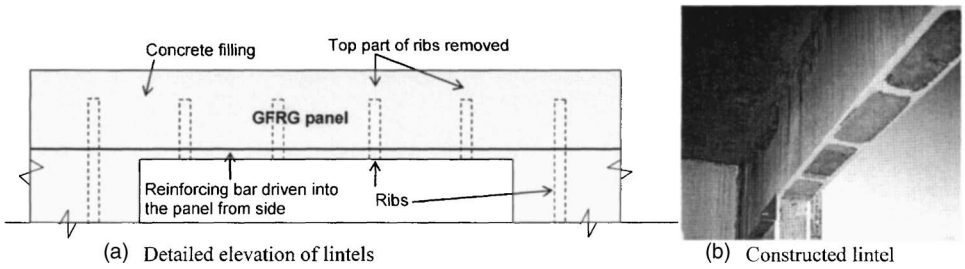

Fig. 3. Lintel construction

Test instrumentation included the load cell that measured the applied load F (including the weight of the spreader beam system) and the linear variable differential transformer (LVDT) that measured the displacement at the bottom of the midspan, as shown in Fig. 5. Testing was conducted under a displacement control mode. In a test, the hydraulic jack at the top of the test rig applied a displacement increment to the specimen. Responses including load and displacement were recorded automatically. The specimen was then visually inspected and cracks were marked. When all the information was obtained for a displacement step, a new displacement increment was applied, and so on. The displacement increment was around 0.5–1 mm, and each loading step took a few minutes.

Observation and Test Results

In a manner similar to RC beams, flexural cracks first appeared midspan at the bottom of the beam and more flexural cracks spread toward the supports as the loading increased. Except for Specimen S4, all of the 300-mm deep lintels failed in flexure. The failure mechanism was similar to that of an underreinforced conventional concrete beam, wherein the flexural cracks at the bottom of midspan opened up followed by the concrete crushing at the top of the beam. The peak load was reached when the concrete crushed. The typical flexural failure mode is shown in Fig. 6. One of the 300-mm deep specimens (S4) failed in shear. This we consider to be due to the bad workmanship involved in either the concrete casting process or in the manufacture of the GFRG panel.

All 550- and 800-mm deep beams failed in a shear mode. The typical shear failure mode is shown in Fig. 7. It was observed that a shear failure might occur at two different locations, one beside the external point load ("first failure plane") and the other beside the internal point load ("second failure plane") shown in Fig. 8. The occurrence of the first or the second failure plane depended on the position of a point load relative to that of a rib inside the lintel. It can be seen from Fig. 8 that the shear force at the first shear plane was $F/2$ and that at the second shear plane was $F/4$. Therefore, the shear force at the first shear plane was always greater than that at the second shear plane. However, when a point load was close to the rib and the shear plane was steep such that shear enhancement became involved, the enhanced shear strength at the first failure plane would be increased. In the case where the enhanced shear strength at the first failure plane exceeds the shear force of $F/2$, a shear failure would occur at the second failure plane. The locations of the shear failure plane for all the specimens are given in Table 3.

Except in a minority of cracks where the glass fibers failed in tension as the cracks widened, most fine flexural cracks closed and disappeared when the specimen was unloaded. Clearly the glass fibers inside the GFRG panel deformed elastically in the loading and unloading process.

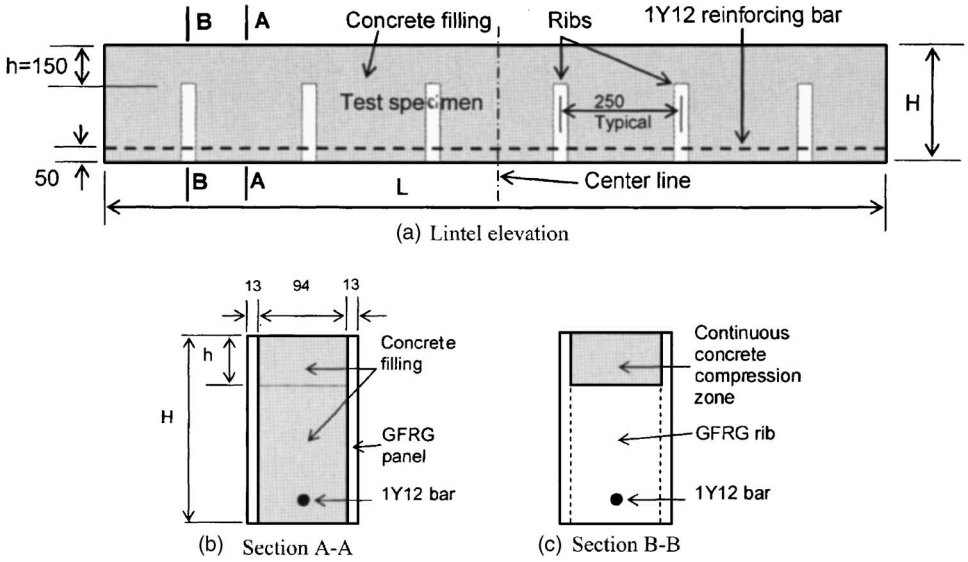

Fig. 4. Details of test specimen

Table 3. Summary of Specimens and Test Results

Specimen	Depth H (mm)	Length L (mm)	Peak load F (kN)	Failure mode	Flexural strength M_u (kN m) or shear strength V_u (kN)
S1	300	600	301.7	Flexural	22.6
S2	300	600	311.0	Flexural	23.3
S3	300	1,200	126.8	Flexural	19.0
S4	300	1,200	95.1	Shear	—
S5	300	1,800	83.6	Flexural	18.8
S6	300	1,800	82.2	Flexural	18.5
S7	550	1,200	282.7	2nd shear plane	70.7
S8	550	1,200	275.9	2nd shear plane	69.0
S9	550	1,800	158.2	2nd shear plane	39.6
S10	550	1,800	138.0	2nd shear plane	34.4
S11	550	2,400	99.2	1st shear plane	49.6
S12	550	2,400	129.3	1st shear plane	64.7
S13	800	1,800	174.1	1st shear plane	87.1
S14	800	1,800	201.8	2nd shear plane	50.5
S15	800	2,400	139.0	1st shear plane	69.5
S16	800	2,400	146.0	1st shear plane	73.0
S17	800	3,000	89.2	1st shear plane	44.6
S18	800	3,000	135.8	1st shear plane	67.9

Analysis of the Test Results

Flexural Strength

The typical response curve for a flexural failure is shown in Fig. 9. As mentioned in the previous section, the flexural failure process was identical to that of the conventional underreinforced RC beams. If it is assumed that (1) the GFRG panel and the infill concrete are fully bonded without relative slip and (2) plane section remains plane, then the conventional RC flexural theory can be used to calculate the flexural strength.

On the basis of these assumptions the ultimate flexural strength of the lintel can be calculated with the model as shown in Fig. 10. The flexural strength of the infill reinforced concrete is modeled by Figs. 10(a–c), whereas that of the GFRG panel is modeled by Fig. 10(d). The ACI 318-02 model or the AS3600 (Australian concrete design code) (SAI 2001) model (both are identical in this case) is used for the RC part. A simplified model of Fig. 10(d) is adopted as the stress block for the GFRG panel. It will be shown later that this simplified model for GFRG panel will not significantly affect the accuracy of the result.

To calculate the flexural strength of the lintels, the following material properties have been determined from the tension and compression material tests (Wu 2002): tensile strength of the

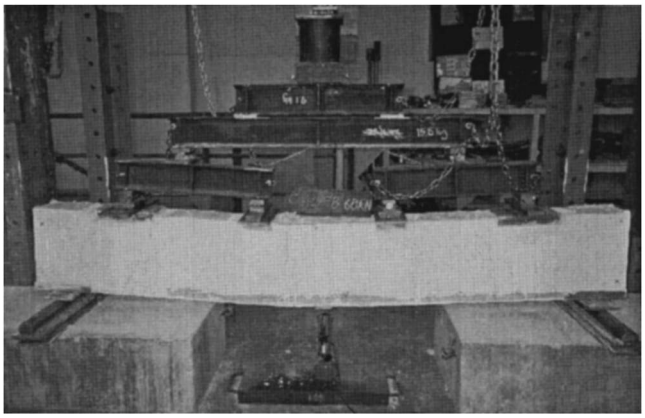

Fig. 6. Typical flexural failure mode

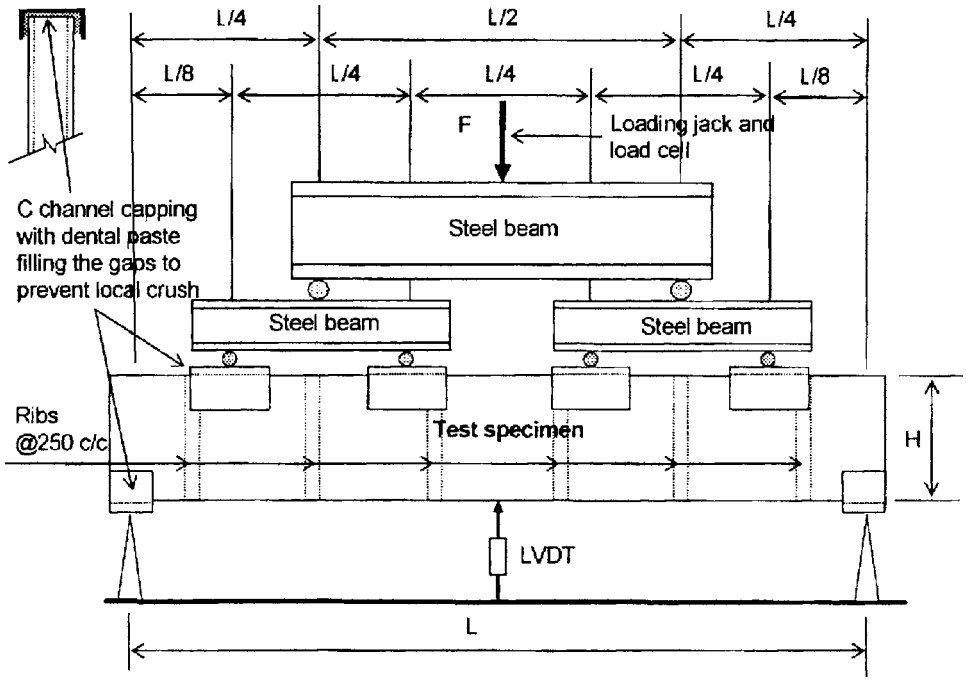

Fig. 5. Test setup

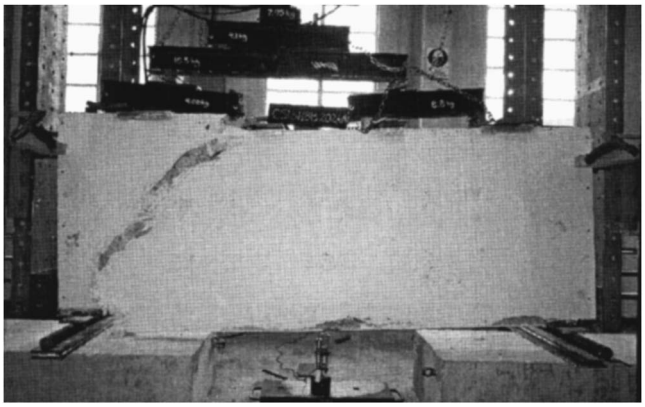

Fig. 7. Typical shear failure mode

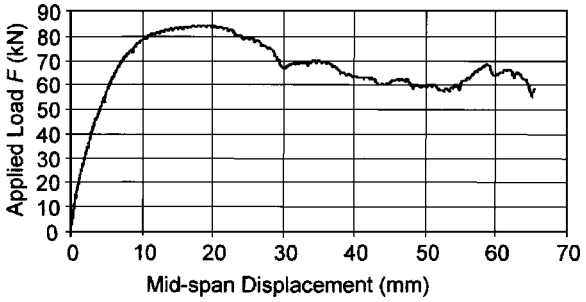

Fig. 9. Typical response with flexural failure (Specimen S5)

GFRG panel f_{wt}=1.9 MPa; compressive strength of the GFRG panels f'_w=5.4 MPa; yield strength of the reinforcing bars f_y=570 MPa; and concrete strength f'_c=21 MPa.

The ultimate moment of the 300-mm deep cross section of the lintels can be calculated by the following simple procedure: from compression force=tension force of the cross section (that is, $F_{cc}+F_{wc}=F_s+F_{wt}$), we have

$$0.85 \cdot f'_c \cdot s \cdot b + 0.85 \cdot f'_w \cdot 2t \cdot s = f_y \cdot A_s + f_{wt} \cdot 2t \cdot (H - x)$$

where F_{cc}, F_{wc}, F_s, and F_{wt}=compressive resistance of concrete and GFRG panel, tensile resistance of steel bar and GFRG panel, respectively, as shown in Fig. 10; s=depth of the compression stress block and $s=0.85 \cdot x$; b=breadth of the concrete compression zone; A_s=area of tension bar; t=skin thickness of GFRG panel; and H=depth of the beam. By substituting the actual strengths and dimensions into the above equation we have

$$0.85 \cdot x \cdot (94 \times 0.85 \times 21 + 2 \times 13 \times 0.85 \times 5.4)$$

$$= 570 \times 113 + 2 \times 13 \times (300 - x) \times 1.9$$

from which the compression zone depth is calculated to be x=50.2 mm. From this compression zone depth it can be verified that the steel bar has yielded. The material partial safety factor is taken as 1 in the above calculation. Taking moment about a point for all forces in the cross section gives M_u=16.6 kN·m.

If the GFRG panel is ignored and only the forces in the concrete and the steel bar are considered, the ultimate moment M_u is calculated to be 14.9 kN·m. Therefore, the moment contribution from the GFRG panel is 16.6−14.9=1.7 kN·m. From the unfilled lintel tests in which no material was filled into the cavities of the GFRG panel, the average moment resistance of the 300-mm deep lintels happened to be 1.7 kN·m (Wu 2002). Both the unfilled lintel test results and the above calculation indicated that the moment contribution from the GFRG panel is small compared to that of the RC part. As a result, the GFRG panel can be ignored in the flexural calculation. This is the reason mentioned earlier that the model of Fig. 10(d) does not significantly affect the flexural strength of the lintels.

It can easily be determined from Fig. 5 that the test peak load F relates to the maximum moment of the beam by the following relation

$$M_u = \frac{1}{8} F \cdot L \tag{1}$$

The experimental moment capacity of the lintels is calculated using Eq. (1); the results are provided in Table 3. The average flexural strength is 18.8 kN·m calculated from the test results of Specimens S3, S5, and S6. Specimen S4 failed in a shear mode, and therefore, cannot be used in this calculation. The flexural strength of Specimens S1 and S2 is not used because these two lintels are considered to be deep beams in which the aspect ratio L/H was 2. For deep beams the flexural design theory shown in Fig. 10 (i.e., the assumption of plane section remaining plane is not applicable). Comparing the test result of M_u=18.8 kN·m to the theoretical result of 16.6 kN·m, the theoretical design model is considered as acceptable.

Shear Strength

The typical response curve of lintels failing in shear is shown in Fig. 11. As expected the response curve shows a sudden drop of load-carrying capacity when the failure occurs. The modeling of shear strength is complicated and inaccurate even for conventional RC beams. Despite the great research efforts all over the world over the past 40 years, there is still not a simple and accu-

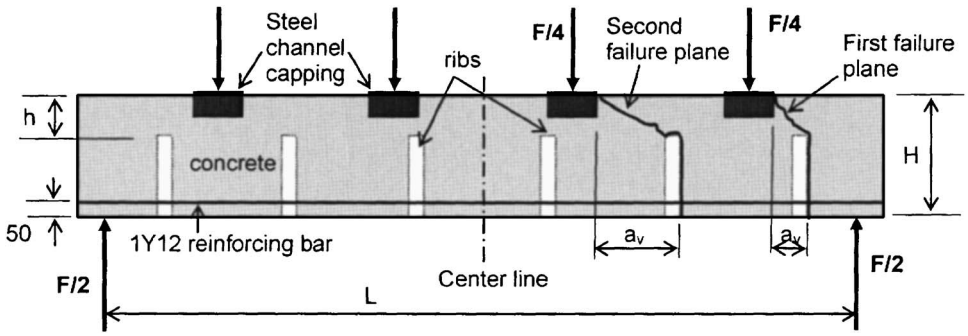

Fig. 8. Shear failure mechanism

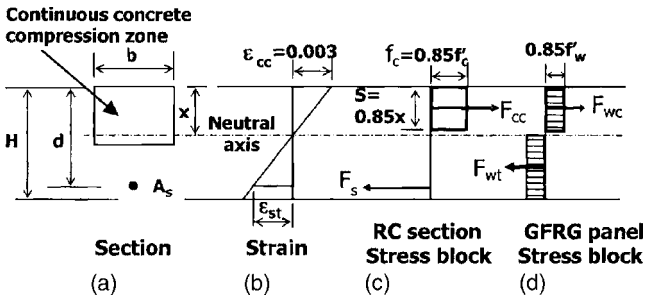

Fig. 10. ACI 318-02 flexural design model

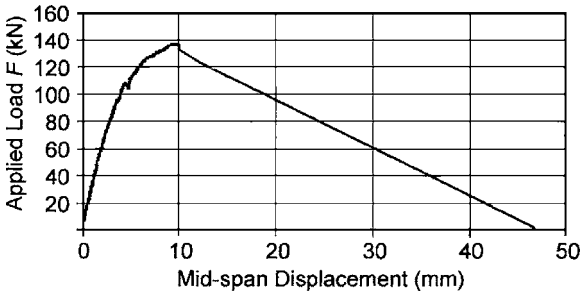

Fig. 11. Typical response for shear failure (Specimen S18)

rate shear strength model for RC beams (Zararis 2003). The composite lintels studied in this work are more complicated than that of the conventional RC beams. Therefore, development of new shear strength model will not only be difficult but also controversial. As a result, the shear strength model in this work is developed by analogy to that of the conventional RC beam.

In a manner similar to the design of conventional RC beams where the shear strength of a beam is split into the concrete shear strength V_c and the stirrup shear strength V_s, the shear strength of the composite lintels can also be separated into two parts: (1) the shear strength due to the infill concrete V_c, as shown in Fig. 12; and (2) the shear strength due to the web reinforcement V_w, as shown in Fig. 13. In this case the web reinforcement is the glass fibers instead of steel stirrups.

The shear strength due to infill concrete may be calculated in a similar way to that of the conventional RC beam. Based on the current shear strength model of the RC beam, the concrete shear strength V_c is composed of three parts: (1) shear resistance from the dowel action of the longitudinal reinforcing bars; (2) aggregate interlocking on the diagonal crack face; and (3) shear force at the compression zone, as shown in Fig. 12(a). Similar to RC beams, these three actions also exist in the infill concrete beam, as shown in Fig. 12(b). However, part of the concrete in contact with GFRG ribs has little shear resistance except some frictional force between the concrete and the GFRG ribs that is negligible. Therefore, the effective depth of the concrete infill beam should be considered as h instead of d, as shown in Fig. 12(b). In other words, the shear strength V_c of the lintel can be calculated with the conventional shear strength model, which would consider the infill concrete as a concrete beam with an effective depth of h.

The shear strength contribution from the GFRG panel can be considered as web reinforcement, as shown in Fig. 13(b). This is because the glass fibers inside the GFRG panel act as web-tension reinforcement in the shear failure plane when a diagonal shear failure occurs. This can be seen in Fig. 7. If we assume a 45° shear failure plane, which is similar to that of RC beams, the shear strength due to the GFRG panel can be calculated with the following equation:

$$V_w = f_{wt} \cdot A_w = f_{wt} H \cdot a_w \tag{2}$$

where f_{wt}=1.9 MPa, the tensile strength of the GFRG panel; A_w=projected area of the GFRG shear plane on the horizontal surface; and a_w=cross-sectional area of GFRG panel of an unit length.

Based on the above shear model, the shear strength of the lintels can be calculated with the existing codes, such as ACI, Eurocode 2, or AS3600. Before calculating the theoretical shear strength of the tested lintels to verify the theory, it is desirable to find the order of error of the existing codes' provisions on the shear strength of concrete for conventional RC beams. Comparisons between test results and theoretical results calculated by existing codes are made in Table 4. The 38 test beams in Table 4 are selected from the 166 test beams without stirrups that were collected by Zararis and Papadakis (2001). The 38 beams are selected because these beams have a similar effective depth to that of the specimens tested in this work. Furthermore, the selected beams also have a low concrete strength of less than 40 MPa, so that the conditions of the selected beams are similar to that of the lintels tested in this work.

In Table 4, the theoretical shear strengths of concrete are calculated by three codes: ACI (simplified method), Eurocode 2, and AS3600, with Eqs. (3)–(5), respectively

$$V_{c\_aci} = \frac{1}{6}\sqrt{f'_c} \cdot b \cdot d \tag{3}$$

$$V_{c\_euro} = \beta \cdot \tau_{RD} \cdot k(1.2 + 40\rho) \cdot b \cdot d \tag{4}$$

$$V_{c\_as} = \beta_1 \beta_3 (\rho \cdot f'_c)^{1/3} \cdot b \cdot d \tag{5}$$

where d=effective depth of beam; τ_{RD}=basic shear strength of concrete provided in Eurocode 2; $\rho = A_s/bd$, the tension reinforcement ratio; $\beta = 2.5d/a_v$, the shear strength enhancement factor under concentrated load, in which a_v=horizontal length of the shear crack as shown in Fig. 8; $k = 1.6 - d/1{,}000 > 1$ (d in mm); $\beta_1 = 1.1(1.6 - d/1{,}000) \geq 1.1$; and $\beta_3 = 2d/a_v$.

For comparison with the test results, the partial safety factor for material is taken as 1 in the above theoretical strength calculations. From Table 4 it can be seen that Eurocode 2 and AS3600 give a similar prediction on the shear strength of concrete for the test beams. The average value of the experimental shear strength over theoretical strength for Eurocode 2 and AS3600 are 1.11 and 1.09, respectively. The theoretical strength by Eq. (3) is not as good as the other two, because both the tension reinforcement and shear enhancement are not considered in the equation. Therefore, only Eqs. (4) and (5) are used to calculate the theoretical strength of concrete of the composite lintels.

The experimental shear strength of the 12 test specimens is calculated and provided in Table 3. As mentioned earlier, the shear strength equals $F/2$ if the beam failed at the first failure plane, and it is $F/4$ when it failed at the second failure plane. It can be seen in Table 3 that the shear strength of the lintels with similar depths varies with the lintel span. This was caused by the shear enhancement [see Eqs. (4) and (5)], which varies with different spans of beams due to the relative position of the point load with respect to that of the nearby rib. This relative position from a point load (top of the shear plane) to a rib of GFRG panel

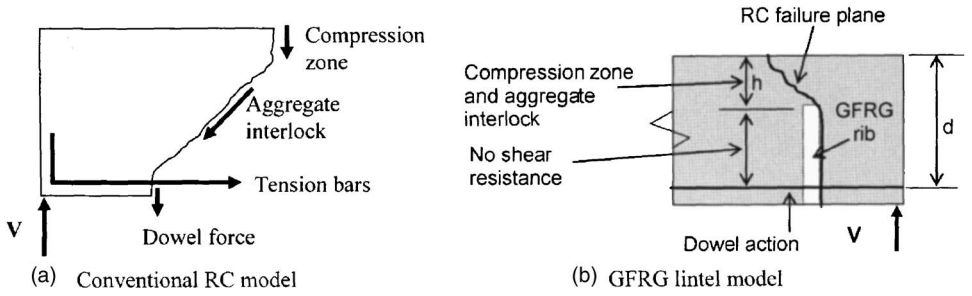

Fig. 12. Shear strength due to concrete

(bottom of the shear failure plane) is determined by the setting out of the point load (see Fig. 5) and the setting out of the ribs [see Fig. 4(a)].

The theoretical strengths of the 12 tested lintels are calculated and compared to that of the test results in Table 5. With the proposed theoretical models, the average value of the experimental shear strength over the theoretical strength is about 1.1, as shown in Table 5. This value is similar to that for conventional RC beams provided in Table 4. Therefore, the proposed shear model is considered to be as good as that for conventional RC beams.

Discussions

Flexural Strength

The difference between the theoretical moment capacity (16.6 kN·m) and the experimental peak moment (18.8 kN·m) is not likely to be caused by the adoption of the simplified rectangular stress block shown in Fig. 10. Nonlinear segmental layered computer modeling (Wu et al. 2004), in which Mander et al.'s (1988) model is used to model the nonlinear concrete stress distribution across the cross section, finds that the ultimate moment of the RC cross section (excluding the GFRG panel) is M_u=15.4 kN·m. This result is close to 14.9 kN·m that was calculated with the rectangular stress block.

Another possible source of error may come from the assumption of full bond between the GFRG panel and the infill concrete. If we assume that the infill RC beam and the GFRG panel act independently (without interaction) and both have sufficient ductility so that the total flexural strength is the sum of the independent moment capacity of the two members, then the total moment resistance will be 14.9 kN·m (RC beam)+1.7 kN·m (GFRG panel)=16.6 kN·m, which happens to be the same as the original theoretical result from the full bond model of 16.6 kN·m. Therefore, the assumption of full bond between the GFRG panel and the infill concrete is not likely to be the major cause of the discrepancy. One of the possible causes of error is the scattering of the material properties and the workmanship (inaccuracy in dimensions, etc.) involved in making the test specimens.

Shear Strength Model

The larger discrepancy between the theoretical and the test results of Specimens 7 and 8 (see Table 5) was caused by the steeper shear plane, because these two lintels were relatively deeper than other shear failed beams (L/d smaller than others). The steeper shear plane changed the diagonal tension shear failure mode in the GFRG panel to shear-compression failure mode, a phenomenon similar to that in conventional reinforced concrete beams (Kong and Evans 1994). Therefore the shear strength due to the GFRG panel predicted by Eq. (2), which is suitable for diagonal tension shear failure, is no longer applicable. However, the shear strength due to diagonal tension failure is smaller than that for shear-compression failure. As a result the shear strength provided by Eq. (2) is conservative and could still be used for design purpose. Further study on this matter is needed.

The shear strength of Specimen S17 is significantly smaller than that of S18, which was identical to S17. Therefore, the lower test strength of S17 was considered to be caused by workmanship involved in making the specimen. It may also be caused by the variability of the GFRG panel. For this reason, a higher strength reduction factor is adopted in shear strength design (see next section).

Design Strength Reduction Factors

For design purpose a strength reduction factor ϕ should be applied to the ultimate strength capacities obtained from the above strength models. The strength reduction factors used for the flexural strength and shear strength are 0.8 and 0.6, respectively (Wu 2002). These factors are generally in accordance with AS 3600-2001, with a modification of shear strength reduction factor from 0.7 to 0.6 considering the less ductile failure mode and the relative short period of application of this new material.

The structural capacity of the composite lintels shall be designed using the following equation

$$S^* \leq \phi R \tag{6}$$

where S^*=design action effect (flexural moment or shear force) due to the design load; and R=load capacity (moment capacity or shear strength) calculated from the relative strength models proposed in this paper.

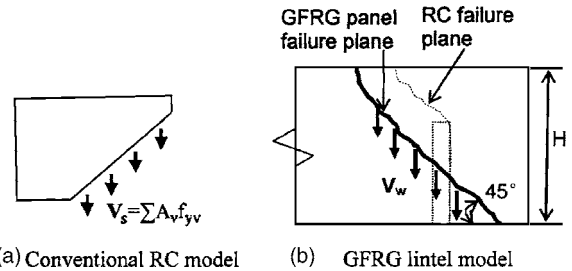

Fig. 13. Shear strength due to web reinforcement

Table 4. Comparison of Shear Strength by Different Codes

Beam number	f'_c (Mpa)	b (mm)	d (mm)	ρ (%)	V_u (kN)	V_{u_aci} (kN)	V_u/V_{u_aci}	V_{u_as} (kN)	V_u/V_{u_as}	V_{u_euro} (kN)	V_u/V_{u_euro}
Leo1	35.9	100	140	1.66	21.6	13.98	1.55	18.92	1.14	21.00	1.03
Leo2	35.9	100	140	1.66	23.7	13.98	1.70	18.92	1.25	21.00	1.13
Leo3	37.7	100	150	1.33	22	15.35	1.43	19.01	1.16	20.91	1.05
Kani1	26.4	152	140	2.59	32	18.22	1.76	30.11	1.06	31.05	1.03
Kani2	28	151	137	2.73	29.1	18.24	1.60	30.44	0.96	30.94	0.94
Kani3	28	152	137	2.73	30.2	18.37	1.64	30.64	0.99	31.14	0.97
Kani4	24.8	151	132	2.85	28.2	16.54	1.70	28.67	0.98	30.43	0.93
Kani5	24.8	151	133	2.81	27.1	16.67	1.63	28.73	0.94	30.45	0.89
Kani6	24.8	152	138	2.69	28.9	17.41	1.66	29.48	0.98	31.15	0.93
Kani7	25.1	151	135	2.89	32.6	17.02	1.92	29.52	1.10	31.34	1.04
Kani8	27.3	153	137	2.67	28	18.25	1.53	30.36	0.92	31.02	0.90
Kani9	26.4	153	139	2.6	31.6	18.21	1.74	30.15	1.05	31.08	1.02
Kani10	27.3	152	138	2.68	28.9	18.27	1.58	30.40	0.95	31.10	0.93
Kani11	20.9	155	139	2.64	39.3	16.42	2.39	28.40	1.38	27.49	1.43
Taylor1	32	60	139	1.35	11.6	7.86	1.48	10.13	1.14	10.73	1.08
Taylor2	32	60	139	1.35	12.1	7.86	1.54	10.13	1.19	10.73	1.13
Taylor3	32	60	139	1.35	10.6	7.86	1.35	10.13	1.05	10.73	0.99
Taylor4	32	60	139	1.35	11.4	7.86	1.45	10.13	1.13	10.73	1.06
Chana1	27.6	100	177	1.77	23.8	15.50	1.54	21.82	1.09	22.04	1.08
Chana2	27.6	100	177	1.77	23.9	15.50	1.54	21.82	1.10	22.04	1.08
Chana3	29.4	100	177	1.77	24.5	16.00	1.53	22.28	1.10	22.04	1.11
Chana4	29.4	100	177	1.77	25.5	16.00	1.59	22.28	1.14	22.04	1.16
Chana5	32.1	100	177	1.77	26.5	16.71	1.59	22.95	1.15	24.97	1.06
Chana6	32.1	100	177	1.77	23.2	16.71	1.39	22.95	1.01	24.97	0.93
Chana7	25.3	100	177	1.77	22.1	14.84	1.49	21.20	1.04	22.04	1.00
Chana8	25.9	100	177	1.77	23.4	15.01	1.56	21.36	1.10	22.04	1.06
Chana9	35.8	100	177	1.77	21.4	17.65	1.21	23.80	0.90	27.18	0.79
Chana10	24.7	60	106	1.78	9.8	5.27	1.86	7.95	1.23	6.88	1.43
Chana11	24.7	60	106	1.78	8.7	5.27	1.65	7.95	1.09	6.88	1.27
Chana12	24.7	60	106	1.78	9	5.27	1.71	7.95	1.13	6.88	1.31
Chana13	24.7	60	106	1.78	9.7	5.27	1.84	7.95	1.22	6.88	1.41
Chana14	32.2	200	170	1.84	47.8	32.16	1.49	44.92	1.06	48.68	0.98
Chana15	32.2	200	170	1.84	47.8	32.16	1.49	44.92	1.06	48.68	0.98
Chana16	31.8	200	170	1.84	55	31.96	1.72	44.73	1.23	48.68	1.13
Chana17	31.8	200	170	1.84	56	31.96	1.75	44.73	1.25	48.68	1.15
Papad1	23.2	200	175	1.15	50.4	28.10	1.79	35.32	1.43	32.86	1.53
Papad2	22.3	200	175	1.15	45.6	27.55	1.66	34.86	1.31	32.86	1.39
Walr1	27.5	200	125	0.83	29.8	21.85	1.36	24.79	1.20	24.99	1.19
Mean							1.62		1.11		1.09

Table 5. Shear Strength of Lintels

Specimen	f'_c (MPa)	b (mm)	d (mm)	ρ (%)	V_u (kN)	V_{u_as} (kN)	V_w (kN)	β_3	V_u/V_{u_as}	V_{u_euro}	V_u/V_{u_euro}
S7	21	94	150	0.8	70.7	48.47	27.20	1.71	1.46	53.17	1.33
S8	21	94	150	0.8	69	48.47	27.20	1.71	1.42	53.17	1.30
S9	21	94	150	0.8	39.6	39.61	27.20	1.00	1.00	42.35	0.94
S10	21	94	150	0.8	34.5	39.61	27.20	1.00	0.87	42.35	0.81
S11	21	94	150	0.8	49.6	48.47	27.20	1.71	1.02	53.17	0.93
S12	21	94	150	0.8	64.7	48.47	27.20	1.71	1.33	53.17	1.22
S13	21	94	150	0.8	87.1	64.32	39.50	2.00	1.35	69.80	1.25
S14	21	94	150	0.8	50.5	51.91	39.50	1.00	0.97	54.65	0.92
S15	21	94	150	0.8	69.5	60.77	39.50	1.71	1.14	65.47	1.06
S16	21	94	150	0.8	73	60.77	39.50	1.71	1.20	65.47	1.12
S17	21	94	150	0.8	44.6	58.11	39.50	1.50	0.77	62.22	0.72
S18	21	94	150	0.8	67.9	58.11	39.50	1.50	1.17	62.22	1.09
Mean									1.14		1.06

Summary and Conclusions

This experimental work investigates the flexural and shear performances of the GFRG composite lintels. Based on the test result, theoretical design models are proposed for both the flexural and shear strengths. Comparison between the test and theoretical results verify the accuracy of these models.

Design of the GFRG composite lintels involves the selection of tension reinforcement bars and the determination of the depth of the continuous compression zone h, as shown in Fig. 4. Conventional flexural design theory for RC beams can be used for the flexural design of the concrete-filled GFRG lintels considering the concrete cross section only and ignoring the GFRG panel. The continuous compression zone depth h should be determined such that the neutral axis does not fall below this zone in order to prevent crushing of gypsum plaster. The depth h is also critical for the shear strength of the composite lintels because it is the effective depth of the effective shear resistance area. The conventional shear model can be used to calculate the shear strength contributed by the infill concrete, assuming an effective depth of h. The shear strength contribution of the GFRG panel comes from the glass fibers that can be considered to be similar to the contribution of stirrups in conventional RC beam, where the tensile strength of the glass fiber is equivalent to that of steel stirrups.

Acknowledgment

The work described in this paper was supported by a grant from City University of Hong Kong (Project No. 7001809).

Notation

The following symbols are used in this paper:

A_s = area of tension reinforcement;
A_w = area of shear failure plane of GFRG panel projected on horizontal plane;
a_v = horizontal length of concrete shear failure plane;
a_w = cross-sectional area of GFRG panel of unit length;
b = breadth of cross section;
d = effective depth of cross section;
f'_c = strength of concrete;
f'_w = compression strength of GFRG panel;
f_{wt} = tensile strength of GFRG panel;
f_y = yield strength of reinforcing bar;
F = total vertical load;
H = depth of beam;
h = depth of continuous compression zone of concrete;
k = $1.6-d/1{,}000>1$ (d in mm);
L = span length (mm);
M_u = ultimate flexural moment of section;
V_c = shear strength contribution from concrete;
V_{c_aci} = concrete shear strength by ACI code;
V_{c_as} = concrete shear strength by AS3600;
V_{c_euro} = concrete shear strength by Eurocode 2;
V_s = shear strength contribution from transverse steel;
V_w = shear strength contribution from glass fiber in GFRG panel;
V_u = experimental shear strength;
V_{u_aci} = theoretical shear strength by ACI code;
V_{u_as} = theoretical shear strength by AS3600;
V_{u_euro} = theoretical shear strength by Eurocode 2;
x = depth of compression zone;
β = $2.5d/a_v$, shear enhancement factor under concentrated load for Eurocode 2;
β_1 = $1.1(1.6-d/1{,}000)\geqslant 1.1$;
β_3 = $2d/a_v$, shear enhancement factor under concentrated load for AS3600;
ε_c = compressive strain;
ε_t = tensile strain;
ρ = A_s/bd, ratio of tension reinforcement; and
τ_{RD} = basic shear strength of concrete from Eurocode 2.

References

Kong, F. K., and Evans, R. H. (1994). *Reinforced and prestressed concrete*, Chapman & Hall, London.

Mander, J. B., Priestley, M. J. N., and Park, R. (1988). "Theoretical stress–strain model for confined concrete." *J. Struct. Eng.*, 114(8), 1804–1826.

Standards Australia International (SAI). (2001). *Concrete structures*, *AS 3600-2001*, Standards Australia International, Sydney, Australia.

Wu, Y. F. (2002). "A 2002 report into the physical testing and the development of design guidelines for the structural application of rapidwall in building construction." *Dare Sutton Clarke Engineers*, Adelaide, Australia.

Wu, Y. F. (2004). "The effect of longitudinal reinforcement on the cyclic shear behavior of glass fiber reinforced gypsum wall panels: Tests." *Eng. Struct.*, 26(11), 1633–1646.

Wu, Y. F., and Dare, M. P. (2004). "Axial and shear behavior of glass fiber reinforced gypsum wall panels: Tests." *J. Compos. Constr.*, 8(6), 569–578.

Wu, Y. F., Griffith, M. C., and Oehlers, D. J. (2004) "Numerical simulation of steel plated RC columns." *Comput. Struct.*, 82(4–5), 359–371.

Zararis, P. D. (2003). "Shear strength and minimum shear reinforcement of reinforced concrete slender beams." *ACI Struct. J.*, 100(2), 203–214.

Zararis, P. D., and Papadakis, G. C. (2001). "Diagonal shear failure and size effect in RC beams without web reinforcement." *J. Struct. Eng.*, 127(7), 733–742.